Neurobiology of Disease 132 (2019) 104607

Contents lists available at ScienceDirect

Neurobiology of Disease

journal homepage: www.elsevier.com/locate/ynbdi

Sex-dependent impaired locomotion and motor coordination in the HdhQ200/200 mouse model of Huntington's Disease

Jessica K. Cao[a], Katie Viray[a], Larry Zweifel[a,b], Nephi Stella[a,b,*]

[a] Department of Pharmacology, University of Washington, Seattle, WA, United States of America
[b] Department of Psychiatry & Behavioral Sciences, University of Washington, Seattle, WA, United States of America

ARTICLE INFO

Keywords:
Huntington's Disease
Mouse models
Excitotoxicity
Neurodegeneration
Polyglutamine disease
Protein aggregation
Behavior

ABSTRACT

Huntington's Disease (HD) is a fatal neurodegenerative disease characterized by severe loss of medium spiny neuron (MSN) function and striatal-dependent behaviors. We report that female HdhQ200/200 mice display an earlier onset and more robust deterioration in spontaneous locomotion and motor coordination measured at 8 months of age compared to male HdhQ200/200 mice. Remarkably, HdhQ200/200 mice of both sexes exhibit comparable impaired spontaneous locomotion and motor coordination at 10 months of age and reach moribund stage by 12 months of age, demonstrating reduced life span in this model system. Histopathological analysis revealed enhanced mutant huntingtin protein aggregation in male HdhQ200/200 striatal tissue at 8 months of age compared to female HdhQ200/200. Functional analysis of calcium dynamics in MSNs of female HdhQ200/200 mice using GCaMP6m imaging revealed elevated responses to excitatory cortical-striatal stimulation suggesting increased MSN excitability. Although there was no down-regulation of the expression of common HD biomarkers (DARPP-32, enkephalin and CB_1R), we measured a sex-dependent reduction of the astrocytic glutamate transporter, GLT-1, in female HdhQ200/200 mice that was not detected in male HdhQ200/200 mice when compared to respective wild-type littermates. Our study outlines a sex-dependent rapid deterioration of striatal-dependent behaviors occurring in the HdhQ200/200 mouse line that does not involve alterations in the expression of common HD biomarkers and yet includes impaired MSN function.

1. Introduction

HD is an inherited neurodegenerative disease with fatal prognosis characterized by progressive motor, cognitive and psychiatric impairments that develop near middle age, with most patients becoming severely debilitated 15 years after symptom onset. This autosomal-dominant disease is caused by an expansion of a glutamine tract (CAG) in exon 1 of the huntingtin gene (*HTT*), resulting in a mutated huntingtin protein (mHtt) that predominantly affects MSN function (Landles and Bates, 2004; Ross and Tabrizi, 2011). Dysfunction, possibly due to excessive excitatory neurotransmission, and deterioration of MSNs leads to striatal-associated behaviors, most often loss of motor control (Walker, 2007).

The genetic basis of this disease led to the development of preclinical mouse models that recapitulate the molecular mechanisms involved in HD pathogenesis. The HdhQ mouse model was developed using gene targeting technology whereby elevated CAG repeats were inserted into the *Hdh* gene, the mouse homolog to the human *HTT* gene (Lin et al., 2001). Thus, in contrast to other HD mouse models, the HdhQ model lacks human DNA and contains a purely murine genome. Furthermore, natural germline alterations in repeat lengths in the HdhQ150 line were leveraged to create several allelic lines with 200, 315 and 350 CAGs in length, providing powerful genetic tools to study how changes in the number of CAG repeats affect the pathological process and behavioral impairments in mice and whether they reliably model human adult-onset HD (Pouladi et al., 2013). Initial aspects of HD pathology and motor dysfunction are detected in the heterozygous 200 CAG line (HdhQ200/+) starting at approximately 12 months of age that reach severe impairment by 18 months of age; however, HdhQ200/+ mice maintain a normal life span of approximately 2 years that does not mimic the reduced life span known to occur in human adult-onset HD (Heng et al., 2010). As expected, the HdhQ315/+ and HdhQ350/+ mouse lines exhibit a more aggressive phenotype than the HdhQ200/+ line, exemplified by earlier and more rapid impairments of locomotor activity and motor coordination and pronounced mHtt striatal aggregates. However, these mice do not show the expected neuropathological indices of HD (Cao et al., 2018; Kumar et al., 2016). Thus, the HdhQ mouse lines represent a powerful genetic tool to study

* Corresponding author at: Department of Pharmacology, University of Washington School of Medicine, Box 357280, Seattle, WA 98195, United States of America.
E-mail address: nstella@uw.edu (N. Stella).

https://doi.org/10.1016/j.nbd.2019.104607
Received 28 May 2019; Received in revised form 2 August 2019; Accepted 4 September 2019
Available online 06 September 2019
0969-9961/ Published by Elsevier Inc.

how changes in the expression of expanded polyglutamine repeats affects mouse behavior and neuropathological disease progression.

We hypothesized that the HdhQ200/200 mouse line might recapitulate select aspects of HD pathogenesis by maintaining CAG copy numbers and increasing its impact through homozygote expression, which would trigger a profound neuropathological progress and reduce life span (Squitieri et al., 2003). Our longitudinal characterization of the behavioral and histopathological impairment of the HdhQ200/200 mouse line indicates sex-dependent behavioral and pathological deficits occurring with a rapid onset and shortened life span associated with impaired MSN function, well-known hallmarks of HD pathogenesis.

2. Materials and methods

2.1. HdhQ200/200 mice colony

Mice were housed in a pathogenic-free facility in accordance with the National Institutes of Health; the Institutional Animal Care and Use Committee at the University of Washington approved all experiments. All mice were maintained on a C57BL/6 genetic background. Female and male heterozygous HdhQ200/+ knock-in mice were mated to produce homozygous (200/200), heterozygous (200/+) and wild-type (+/+) littermates. Animals were housed in cages grouped by sex and mixed genotype, had *ad libitum* access to food and water and were on a 12-h. light/dark cycle. Genotyping was performed with tail snips using primers "cccattcattgcccttgctg" and "gcggctgaggggttga" with a SimpliAmp Thermal Cycler (Thermo Fisher Scientific, Bothell, WA). Moribund stage was indicated by mice displaying tremors, hunching, staggered gait, and inactivity.

2.2. HdhQ200/200 behavioral studies

Balanced cohorts of males and females were used for behavioral studies. Naïve mice were used at all time points (6, 8, 10 and 12 months) and then sacrificed for immunohistochemistry. A complete table of number of animals used for behavioral tests is provided in Supplementary Table 1. All behavioral studies were performed during the light phase of the light/dark cycle, between 9 am and 4 pm. Cages and equipment were thoroughly cleaned with 70% ethanol and dried with a paper towel between trials. Grip strength was measured by recording the latency to fall when animals were placed on a wire cage top and then inverted. A maximum score of 90 s. was used. Rotarod (Med Associates Inc., St. Albans, VT) testing included 7 consecutive trials, separated by 15 min resting periods. The rotarod rotational speed used for testing trails began at 4 rpm and increased to 40 rpm for a maximum of 5 mins., with an acceleration of 0.2 rpm per every 4 s. The Phenotyper (Noldus, Wageningen, the Netherlands) testing consisted of 72 h. trials where animals were individually housed in 30 cm × 30 cm Plexiglas cages with access to water, food and housing. A vertically mounted camera continuously tracked animal movement and digital traces were analyzed in Ethovision XT 9.

2.3. Immunohistochemistry

Mice were euthanized with ketamine/xylazine and perfused with 20 ml PBS, followed by 10 ml 4% paraformaldehyde. Brains were extracted and post-fixed in 4% paraformaldehyde overnight at 4 °C. Brains were then dehydrated (first in 15% sucrose and then 30% sucrose for 24 h each) and frozen over dry ice. Coronal sections were cut to a thickness of 30 μm using a sliding microtome and placed in cryoprotectant for storage at −20 °C. IHC analysis of each time point group was processed and stained in parallel. For staining, 2 slices per animal were removed from cryoprotectant, washed 3xPBS and incubated for 90 min at room temperature in blocking buffer (PBS, 5% goat serum, 1% Triton x-100). Slices were then transferred to primary staining solutions (PBS, 2.5% goat serum, 0.5% Triton x-100) for 48–72 h. at 4 °C. Sections were then washed 8xPBS-T and secondary staining was performed using Alexa secondary antibodies at a dilution of 1:500 (PBS, 2.5% goat serum, 0.5% Triton x-100) for 1 h. Additional slices were stained only with secondary staining solutions to serve as non-specific secondary background staining. After secondary staining, sections were washed 6xPBS-T, 1xPBS, mounted on slides and allowed to dry at room temperature overnight. Coverslips were added and sealed with Fluoromount (Sigma, St. Louis, MO) and nail polish.

2.4. Antibodies

The following antibodies were used in this study: CB_1 receptor (L15 pAb guinea pig, gift from Dr. Ken Mackie); synaptophysin (mouse, Synaptic Systems 101011); DARPP-32 (rabbit, Abcam ab40801); DAPI (Invitrogen D3571); ENK (rabbit, Millipore AB5024); vGLUT2 (rabbit, Invitrogen 42-7900); vGAT (mouse, Synaptic Systems 131011); PSD-95 (rabbit, Cell Signaling Technology 3450S); GFAP (mouse, Millipore AB5541); GLT-1 (mouse, gift from Dr. David Cook (Sullivan et al., 2004; Woltjer et al., 2010)); mHtt (N-18) (goat, Santa Cruz Biotechnology (Mitsui et al., 2002)); 1C2 (mouse, Millipore 1574); Alexa Fluor 488/555/647 (goat/donkey, ThermoFisher).

2.5. Microscopy

Images were collected on a Marianas microscope (Intelligent Imaging Innovations, Inc. Denver, CO) equipped with either 20×/0.75 NA or 40×/0.75 NA air objective lens with CoolSnap HQ cooled monochrome camera (Photometrics, Tucson, AZ) as *Z*-stacks of 10 at the NIDCD Research Core Center at the University of Washington. Four images were collected from each animal of the dorsal lateral striatum. Noise reduction of images was achieved by deconvolution of Nearest Neighbors using SlideBook (Intelligent Imaging Innovations, Inc., Denver, CO). Exposure times were optimized for each antibody to ensure that > 99% pixels were within the linear range. HdhQ200/200 and wild-type samples were imaged at the same exposure and laser settings to ensure consistency and accurate comparison. Excitation laser of 403 nm was used to excite DAPI, FITC to excite Alexa 488, Cy3/TRITC to excite Alexa 555, and FarCy5 to excite Alexa 647.

2.6. Semi-quantitative image analysis and statistics

All images were analyzed using ImageJ (National Institutes of Health) with custom written macros. Macros were applied blindly to each batch of images and analyzed as previously reported by our laboratory (Horne et al., 2013). Each z-stack was flattened into one image of average or maximum pixel intensity and each channel was split into an individual image. The mean intensity and standard deviation of each fluorophore was measured, and background signal was removed by thresholding images to mean + standard deviation, corresponding to the top third brightest pixels in the Gaussian distribution. After thresholding, final measurements were made by taking the mean intensity of the remaining pixels or by calculating the area of expression. To quantify mHtt aggregation, maxima points above the noise threshold of mean + standard deviation were quantified. Aggregation size was measured by pixel size and all values were normalized to the respective wild-type littermate average.

2.7. In vivo calcium imaging

Two weeks following viral injection surgery (AAV-CAG-GCaMP6m, 3×10^{12} particles/ml, 0.5 ml bilateral), HdhQ200/200 and wild-type littermates were deeply anesthetized with urethane (1 g/kg, i.p.) and placed in a stereotaxic frame. Fluorescence images were acquired by a scanning confocal microscopy coupled to a fiber-optic probe (Mauna Kea Technologies). Spontaneous calcium dynamics were imaged for 5 mins. (12 Hz scan rate) prior to electrical stimulation. To evoke

activation of the striatum, antidromic stimulation of direct pathway fibers from the substantia nigra pars reticulata was first performed. Images were acquired for 5 s to establish baseline fluorescence, followed by electrical stimulation from a bipolar stimulating electrode (400 μmA, 0.5 s. at 60 Hz) with an additional 15 s. of imaging as described (Soden et al., 2013). Data was analyzed offline using ImageCell software (Mauna Kea Technologies) and MatLab as described (Soden et al., 2013).

2.8. Immunoblotting

Mice were euthanized *via* cervical dislocation and brains immediately removed and rinsed in ice cold PBS. Striata were then dissected on ice and flash frozen in liquid nitrogen. Tissue was homogenized in RIPA Buffer (Santa Cruz Biotechnology, Dallas, TX) using a Dounce homogenizer on ice then followed by sonication. Proteins levels were measured using a BCA assay and 20–25 μg protein was loaded were lane. Gels were transferred to PVDF, blocked with Licor Odyssey Blocking Buffer (LI-COR, Lincoln, NE), and stained overnight with primary antibodies prepared in TBS solution containing 5% BSA and 0.02% NaN_3. Secondary staining was carried out in TBS containing 5% BSA at room temperature and blots were imaged and analyzed with fluorescence. Analysis of mHtt size was not feasible, as mHtt protein remained in the stacking gel due to its large size.

2.9. Statistical analyses

Statistical analyses and graphs were generated using GraphPad PRISM 6 (San Diego, CA). Grubbs' test was used to detect any outliers. A chi-square test was used for Mendelian frequencies. Behavioral and biochemical data were analyzed for normal distribution with the Shapiro-Wilk or Kolmogorov-Smirnov normality test, depending on the N. Two-way ANOVA was used to compare behavioral and calcium imaging measurements with a Bonferroni post-hoc analysis. Student's *t*-test was used for immunohistochemical and calcium imaging analysis. Mann-Whitney test was used for nonparametric data sets. Data were considered significant if $p < .05$.

3. Results

3.1. Sex-dependent loss of total body mass and grip strength with shortened life span in HdhQ200/200 mice

HdhQ200/200 mice were generated by breeding HdhQ200/+ x HdhQ200/+ mice, which resulted in litter sizes of 6.9 ± 2.7 pups ($n = 39$ litters), with 23% homozygote, 45% heterozygote and 33% wild-type mice. This ratio deviates from the expected Mendelian ratio of 1:2:1 (χ^2 (2, $N = 3$) = 10.460, $p = .01$) and suggests increased lethality of homozygote embryos. Mice were periodically sequenced to monitor CAG repeat numbers and breeders were strategically chosen to maintain CAG repeats close to an average of 215 (Supplementary Fig. 1). HdhQ200/200 mice of both sexes exhibited overall normal observed behaviors in their home-cage environment and all HdhQ200/200 mice reached moribund stage by approximately 12 months of age (see Materials and methods). This result shows that both sexes in the HdhQ200/200 mouse line exhibit a shortened life span.

We measured total body mass in HdhQ200/200 mice compared to respective wild-type littermates from 6 to 12 months of age and found significant differences between genotypes in both sexes (female: $F_{(1, 51)} = 99.91$, $p < .001$; male: $F_{(1, 56)} = 39.03$, $p < .001$). Post-hoc analyses showed significant differences starting at 6 months of age in female HdhQ200/200 mice, whereas male HdhQ200/200 mice weighed less than wild-type male littermates only at 12 months of age (Fig. 1A, B; the number of animals for each behavioral test is provided in Supplementary Table 1). Combined, these results suggest a more rapid loss in total body mass in HdhQ200/200 females than HdhQ200/200 males, indicative of a more aggressive pathology occurring in females.

As muscle atrophy is a common symptom in HD patients and mouse models, we measured grip strength in HdhQ200/200 mice and wild-type littermates with the inverted wire test (Rogers et al., 1997). Female HdhQ200/200 mice showed a significant decrease in grip strength at 10 and 12 months of age compared to female wild-type littermates ($F_{(1, 51)} = 28.71$, $p < .001$). In contrast, male HdhQ200/200 mice did not exhibit reduced grip strength compared to male wild-type littermates, even though these mice were reaching end-stage of the disease and close to their moribund stage (Fig. 1C, D). Together, these results show rapid disease progression in the HdhQ200/200 mouse line that is more pronounced in females compared to males. Based on this result, we focused our study on mice that were 8 and 10 months old, representative of early and pronounced phases of the disease progression, respectively.

3.2. Sex-dependent reduction in spontaneous locomotion and loss motor coordination in HdhQ200/200 mice

Using the Noldus PhenoTyper, an automated home-cage monitoring system (Cao et al., 2018; Steele et al., 2007), we measured spontaneous locomotion over 72 h. and tested for differences in daily pattern. We found that both male and female HdhQ200/200 mice studied at 8 months of age exhibit decreased spontaneous locomotion during the 12 h. dark phase (when mice are more active) compared to littermate controls (female: $p = .001$; male: $p = .018$) (Figs. 2A, B). At 10 months of age, male HdhQ200/200 mice also showed a significant reduction in dark phase activity, whereas reduction in spontaneous locomotion did not reach significance in female HdhQ200/200 mice (Fig. 2B). When analyzing spontaneous locomotion during the light phase (when mice are less active), we found that female HdhQ200/200 mice show reduced activity compared to their respective wild-type littermates at 8 months of age ($p = .001$) yet male HdhQ200/200 were not significantly different their wild-type littermates at either age (Fig. 2C, D). Note that HdhQ200/200 mice of both sexes did not show changes in activity during the first hour of being placed into the PhenoTyper chamber (an index of novel environment exploration (Steinbach et al., 2016)) when compared to respective wild-type littermates (Fig. 2E, F). These results indicate that HdhQ200/200 mice, especially female HdhQ200/200 mice at 8 months of age, are less active during both the dark and light phase periods compared to wild-type mice, and that this impairment is not apparent during initial novel environment exploration, suggesting that not all modalities involved in spontaneous locomotion are affected.

Impaired motor coordination is a characteristic symptom in HD patients and often measured on an accelerating rotarod in HD mouse models (Pouladi et al., 2013; Walker, 2007). Specifically, impaired motor coordination in mice results from dysfunction of the corticostriatal loop involved in the acquisition of new motor skills and can be measured by comparing the daily averages of mice's latency to fall over multiple trials tested during consecutive days (for example 2 days of rotarod testing with 7 trials each day) (Costa et al., 2004). At 8 months of age, the average latency to fall from the rotarod when averaging the performance measured in 7 trials during the first day of testing was significantly shorter in female HdhQ200/200 mice compared to female wild-type littermates ($p = .02$) and unaffected in male HdhQ200/200 mice, suggesting a sex-dependent impairment (Fig. 3A). Accordingly, a finer analysis of the data gathered at 8 months of age indicated significant differences in Day 1 of rotarod testing ($F_{(1, 84)} = 28.15$, $p < .0001$), with the biggest impairment on trials 2 and 4 in only female HdhQ200/200 mice (Fig. 3B, C). At 10 months of age, the average latency to fall from the rotarod during Day 1 of testing was shorter in female HdhQ200/200 mice compared to female wild-type littermates ($p = .001$) and remained similar between male HdhQ200/200 mice and wild-type littermates (Fig. 3D). A finer analysis of the data gathered at

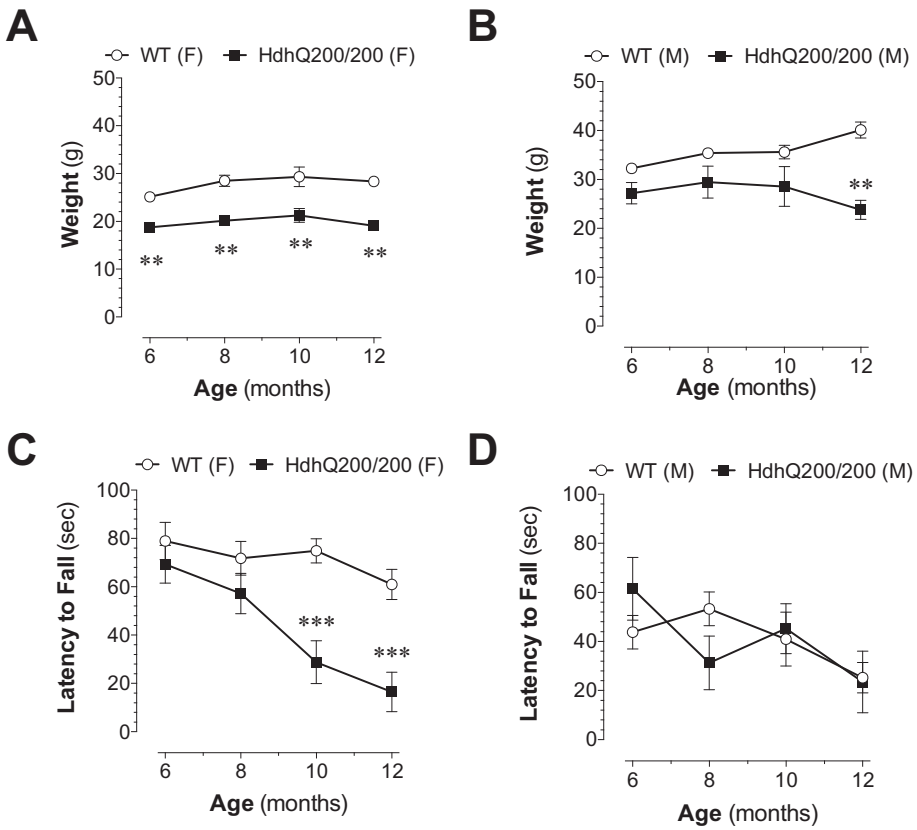

Fig. 1. Weight and grip strength analysis at 6, 8, 10, and 12 months of age in HdhQ200/200 and wild-type mice. (A) Female and (B) male HdhQ200/200 show reduced weight when compared to respective wild-type littermates from age 6 to 12 months. While (C) female HdhQ200/200 mice show progressive grip strength loss starting at 10 months of age when compared to female wild-type littermates, (D) male HdhQ200/200 mice show similar levels to male wild-type littermates. $N = 5–12$ for all groups. Error bars represent S.E.M. and $^{**}p < .01$ and $^{***}p < .001$, with two-way ANOVA with Bonferroni post-hoc test.

10 months of age indicated impairment in female HdhQ200/200 mice compared to female wild-type littermates during both days (Day 1: $F_{(1, 91)} = 84.66$, $p < .001$; Day 2: $F_{(1, 91)} = 14.28$, p = .001), with significant differences in trials 1–4 and 7 on Day 1 (Fig. 3E). Male HdhQ200/200 mice also showed significant differences compared to male wild-type littermates during both days when performing a similar overall analysis (Day 1: $F_{(1, 91)} = 12.78$, p = .001; Day 2: $F_{(1, 91)} = 4.294$, $p = .04$), but no significant difference was found between individual trials (Fig. 3F). These results show a more pronounced deterioration of motor coordination in female HdhQ200/200 mice compared to female wild type mice, whereas male HdhQ200/200 mice exhibit much more subtle impairments compared to male wild-type littermates.

3.3. Sex-dependent accumulation of mHtt aggregates and changes in MSN biomarkers in the striatum of HdhQ200/200 mice

To better understand the sex-dependent deterioration of spontaneous locomotion and motor coordination measured in HdhQ200/200 mice at 8 months of age, we used semi-quantitative immunohistochemistry (sqIHC) to measure the expression of biomarkers known to decrease during HD pathogenesis in the striatum (Cao et al., 2018; Naydenov et al., 2014). First, we verified expression of mHtt and detected many mHtt-aggregated foci in the dorsal striatum of HdhQ200/200 mice of both sexes (Fig. 4A, B) (Mitsui et al., 2002). We then quantified the number of aggregates and found remarkably higher numbers in HdhQ200/200 males compared to HdhQ200/200 females over respective wild-type littermates (female: $p = .016$; male: $p = .008$) (Fig. 4C, D). These results were verified by western blot analysis using an antibody that recognized large polyQ tracts (Trottier et al., 1995) (Supplementary Fig. 2A). Aggregates were uniform in size between female and male HdhQ200/200 mice (Supplementary Fig. 2B) and appeared predominantly as cytoplasmic aggregation foci (AF) that do not overlap with nuclear staining, as previously described in HdhQ200/200 + mice (Fig. 4B) (Heng et al., 2010). Together, these results show that the mHtt protein with extended CAG repeats are expressed and aggregate in the HdhQ200/200 mouse line and differentially accumulate in a sex-dependent manner.

To determine if overt MSN loss occurs in HdhQ200/200 mice at 8 months of age, we measured expression of DARPP-32 in the dorsal striatum of wild-type and HdhQ200/200 mice, as this protein is a dopamine- and cAMP-regulated neuronal phosphoprotein commonly used as a marker of MSNs (Svenningsson et al., 2004). We found significant reduction in DARPP-32 expression in male HdhQ200/200 mice compared to male wild-type littermates ($p = .016$), but not significant in female HdhQ200/200 mice ($p = .068$) (Fig. 4E and F). We then determined if the indirect pathway is affected in the HdhQ200/200 mouse line and measured enkephalin (ENK) expression in the globus pallidus, the output of indirect pathway MSNs. We found that ENK expression was unchanged in both sexes between genotypes (Fig. 4G, H). Together, these results suggest that impairment in spontaneous locomotion and motor coordination measured in female HdhQ200/200 mice at 8 months of age coincides with no overt loss in MSN biomarkers despite mHtt expression.

3.4. Impaired intracellular calcium dynamics in MSN of female HdhQ200/200 mice

We then assessed the functionality of MSNs by measuring their dynamic calcium response *in vivo* following cortical stimulation, as MSN excitability is known to increase in several HD mouse models (Jiang et al., 2016; Miller and Bezprozvanny, 2010; Raymond, 2017). Thus, we utilized *in vivo* calcium imaging to determine if the activity-dependent changes in MSN intracellular calcium concentrations ($[Ca^{2+}]i$) are changed in female HdhQ200/200 mice at 8 months of age compared to wild-type littermates. Specifically, wild-type and HdhQ200/200 female mice were injected with AAV1-GCaMP6m at 7.5 months of age and imaged 2–3 weeks later using a fiber-optic

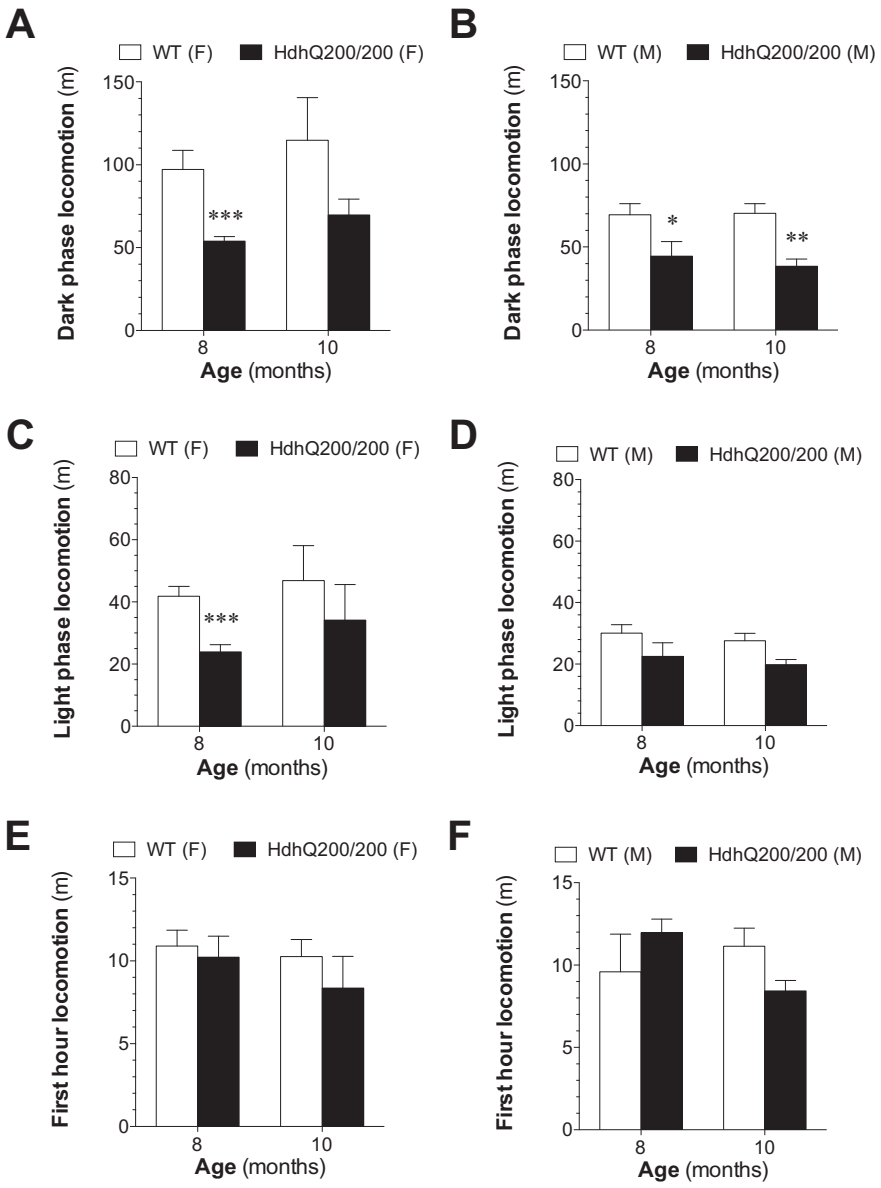

Fig. 2. Decreased spontaneous locomotor activity in the HdhQ200/200 mouse line. Mice were individually housed and spontaneous locomotor activity monitored for 72 h. Both (A) female and (B) male HdhQ200/200 mice had reduced spontaneous dark phase locomotor activity when compared to respective wild-type littermates at 8 and 10 months of age. (C) Female and (D) male HdhQ200/200 mice also showed differences in spontaneous light phase locomotor activity when compared to respective wild-type littermates at 8 and 10 months of age. Neither (E) female nor (F) male HdhQ200/200 differed in exploration during the first hour of a novel environment when compared to respective wild-type littermates. $N = 3–9$ for all groups. Error bars represent S.E.M. and $^{*}p < .05$, $^{**}p < .01$ and $^{***}p < .001$ with two-way ANOVA with Bonferroni post-hoc test.

confocal microscope to visualize fluorescence emitted by the genetically-encoded calcium indicator GCaMP6m in the dorsal striatum and in response to electrical stimulation of the motor cortex (Fig. 5A). Upon stimulation of the motor cortex with a validated protocol (one stimulation of 400 μA at 60 Hz and for 0.5 s) (Soden et al., 2013), we detected an approximately equal number of responsive cells in wild type mice ($n = 11/45$ cells, $n = 5$ mice) and HdhQ200/200 ($n = 12/52$ cells, n = 5 mice). However, the evoked calcium signals were remarkably greater and more prolonged in HdhQ200/200 mice ($F_{(183, 3843)} = 2.91$, $p < .001$), reaching nearly 10-fold larger responses than in wild-type littermate controls ($p = .04$) (Fig. 5B, C). This exaggerated response suggests hyperexcitability and a severe disturbance in calcium signaling in MSN of female HdhQ200/200 mice that occurs as early as 8 months of age.

3.5. Sex-dependent reduction in the expression of the astrocytic protein GLT-1 in HdhQ200/200 mice

To better understand the increased calcium response measure in female HdhQ200/200 MSNs at 8 months of age, we analyzed the striatal expression of several pre- and postsynaptic proteins involved in excitatory transmission, as well as proteins known to handle glutamate and $[Ca^{2+}]i$. First, to determine the integrity of the pre-synapse, we measured the expression of synaptophysin (a key component of presynaptic machinery for neurotransmitter release), CB_1R (presynaptic G protein-coupled receptors that control neurotransmitter release), vGLUT2 (vesicular glutamate transporter 2) and vGAT (vesicular GABA transporter). To determine the integrity of the post-synapse, we measured PSD-95 (postsynaptic scaffolding protein). While these markers are decreased in HD patients and multiple HD model systems (Glass et al., 1993; Goto and Hirano, 1990; Naydenov et al., 2014), their expression was not significantly affected in HdhQ200/200 mice of both sexes (Supplementary Fig. 3A–E). Next, we investigated $[Ca^{2+}]i$ handling by measuring the expression of Orai1 (an essential subunit of the CRAC channel, vital for refilling intracellular calcium stores and promoting neuronal excitability (Dou et al., 2018; Moccia et al., 2015; Prakriya et al., 2006)) and found no change in its expression either (Supplementary Fig. 3F). Lastly, evidence shows that glutamate clearance is decreased in the striatum of HD patients and several HD mouse models (Arzberger et al., 1997; Lievens et al., 2001). Based on this premise, we wondered if the expression of GLT-1 (a subtype of astrocytic glutamate transporter that is predominantly responsible for

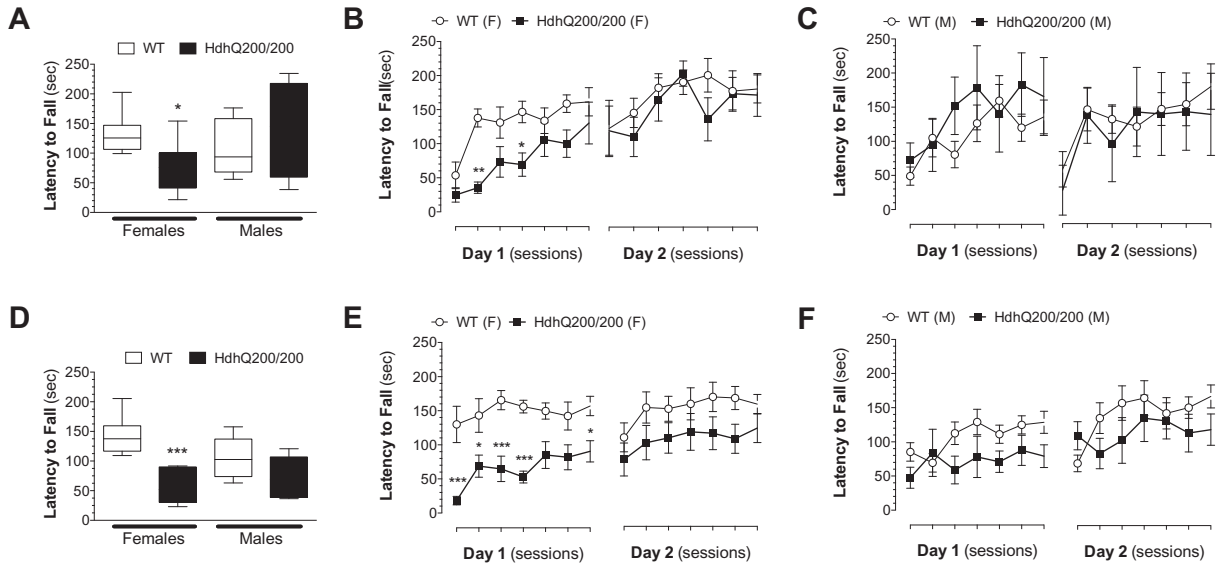

Fig. 3. HdhQ200/200 female mice have early motor coordination impairments. Mice were tested on an accelerating rotarod for 7 sessions for 2 days. (A) At 8 months of age, only female HdhQ200/200 mice show reduced average latency to fall when compared to respective wild-type littermates. (B) Female HdhQ200/200 have a shorter latency to fall during Day 1 of testing. (C) Male HdhQ200/200 report similar latencies to fall when compared to respective wild-type littermates at 8 months of age. (D) At 10 months of age, only female HdhQ200/200 mice show reduced average latency to fall when compared to respective wild-type littermates. Both (E) female and (F) male HdhQ200/200 have shorter latency to fall on all days of testing when compared to respective wild-type littermates. $N = 4$–10 for all groups. Error bars represent S.E.M. and $^{*}p < .05$, $^{**}p < .01$ and $^{***}p < .001$, with two-way ANOVA with Bonferroni post-hoc test or Student's *t*-Test.

glutamate clearance from the synaptic cleft (Perego et al., 2000)) is altered in the HdhQ200/200 mouse line. Remarkably, we measured a 50% reduction in expression of striatal GLT-1 in female HdhQ200/200 mice when compared to female wild-type littermates ($p = .04$) (Fig. 6A–C) and no change in GLT-1 expression between male HdhQ200/200 mice and male wild-type littermates (Supplementary Fig. 4A). Because GLT-1 is an astrocytic-specific transporter, we then explored the possibility that HdhQ200/200 mice exhibit a sex-specific change in astrogliosis. Interestingly, HdhQ200/200 female mice express comparable levels of striatal GFAP to female wild-type littermates

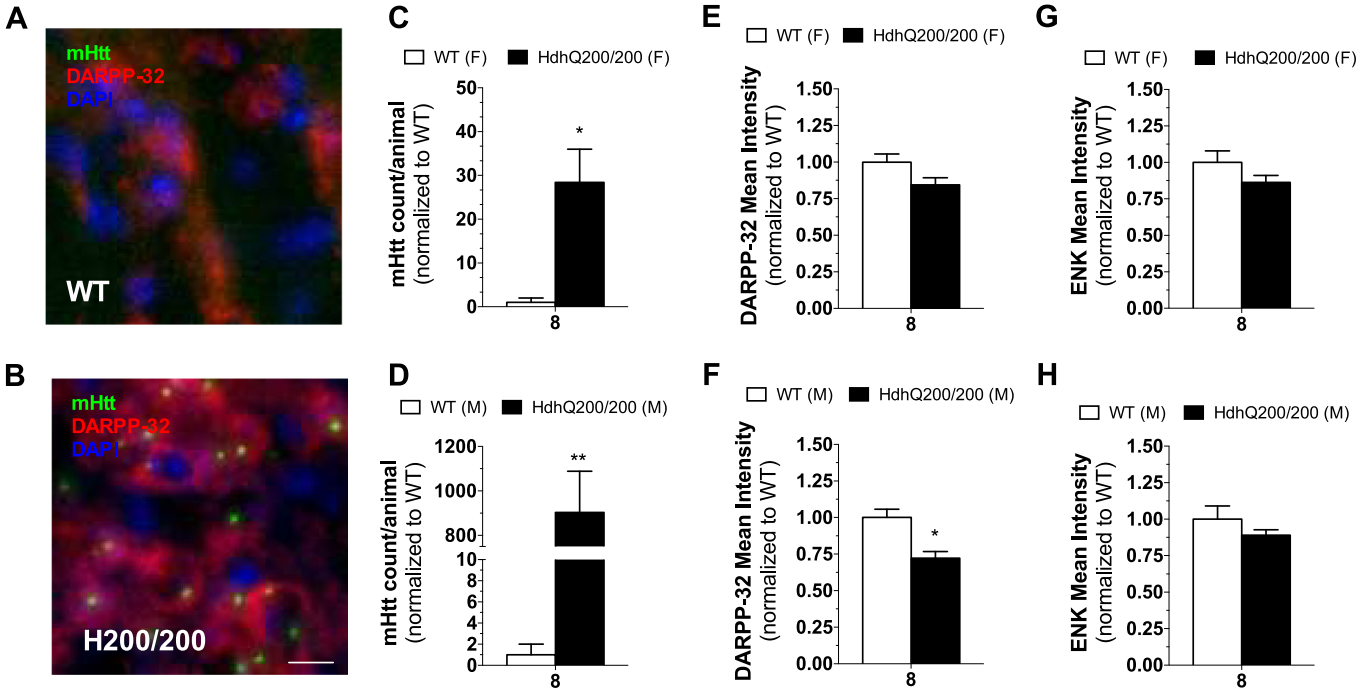

Fig. 4. mHtt aggregation and neuronal loss in the striatum of HdhQ200/200 mice. Representative images of co-staining with DAPI (blue), DARPP-32 (red) to mark striatal MSNs and mHtt aggregates (green), in which no detection was found in (A) wild-type mice but detected in (B) HdhQ200/200 mice at 8 months of age. This is quantified in (C) females and (D) males at 8 months. (E) Female HdhQ200/200 mice do not show reduced DARPP-32 expression at 8 months of age, while (F) male HdhQ200/200 mice do when compared to respective wild-type littermates. Both (G) female and (H) male HdhQ200/200 mice show similar levels of ENK expression at 8 months of age compared to respective wild-type littermates. $N = 4$–5 for all groups. Error bars represent S.E.M. and $^{*}p < .05$ and $^{***}p < .001$, with Student's *t*-Test. Scale bar denotes 25 μm. (For interpretation of the references to color in this figure legend, the reader is referred to the web version of this article.)

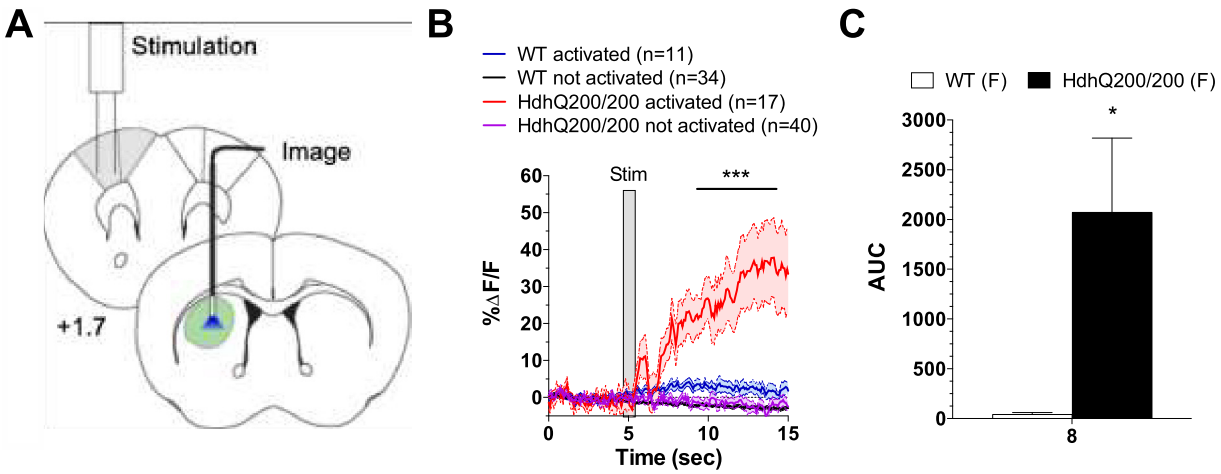

Fig. 5. HdhQ200/200 female mice have abnormal calcium dynamics in striatal neurons in response to cortical stimulation at 8 months of age. (A) Schematic representation of bi-polar stimulating electrode placement in motor cortex (grey) and fiber-optic in dorsolateral striatum (green) (B) Average changes in GCaMP6 fluorescence intensity in the dorsolateral striatum after motor cortex stimulation at 5 s in wild-type and HdhQ200/200 female mice at approximately 8 months of age. (C) Average area under the curve of the fluorescence signal for activated cells from wild-type and HdhQ200/200 female mice. $N = 5$ for all groups. Error bars represent S.E.M. and $*p < .05$ and $***p < .001$, with two-way ANOVA with Bonferroni post-hoc test or Student's *t*-Test. (For interpretation of the references to colour in this figure legend, the reader is referred to the web version of this article.)

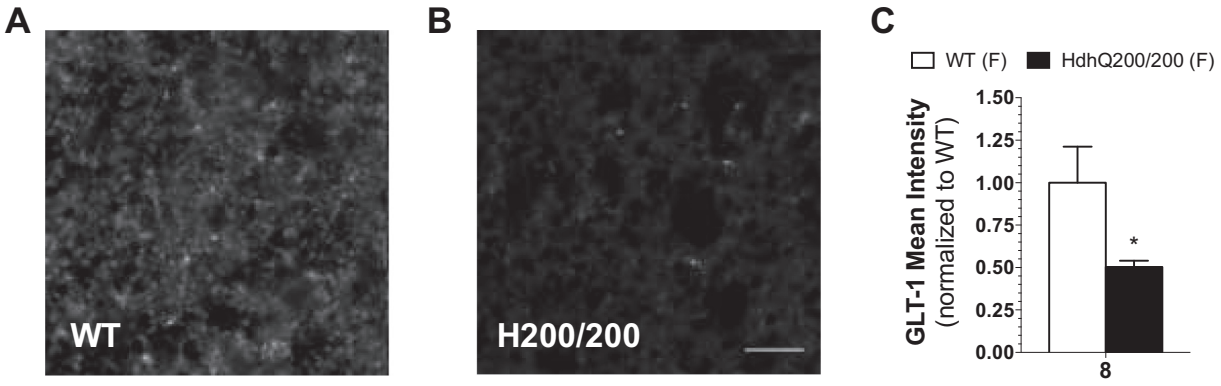

Fig. 6. Expression of striatal GLT-1 is altered in female HdhQ200/200 mice compared to wild-type mice. Representative images of GLT-1 expression in the striatum of female (A) wild-type and (B) HdhQ200/200 mice at 8 months of age. (C) GLT-1 expression is significantly reduced in HdhQ200/200 females compared to wild-type females. $N = 5$ for all groups. Error bars represent S.E.M and $*p < .05$ with Student's *t*-Test. Scale bar denotes 25 μm.

whereas the expression of this astrocytic marker was greater in male HdhQ200/200 mice than male wild-type littermates ($p = .01$) (Supplementary Fig. 4B, C). Together, these results suggest decreased clearance of glutamate due to a reduction in astrocytic GLT-1 expression occurs in HdhQ200/200 females at 8 months of age with no evidence of overt reactive astrogliosis.

4. Discussion

We report a sex-dependent, early onset, deterioration of spontaneous locomotion and motor coordination in the HdhQ200/200 mouse line that coincides with decreased astrocytic GLT-1 expression. We also found several striking dissociations between changes in histopathology biomarkers and behavior. Notably, male HdhQ200/200 mice reached moribund stage by approximately 12 months of age and yet do not lose grip strength, indicating that this behavioral readout does not provide a reliable index of life span and might be related to perseveration, a typical aspect of cognitive change in HD patients and some HD mice (Soloveva et al., 2018). Another striking dissociation was a significant loss in DARPP-32 expression and increase in GFAP expression in the striatum of male HdhQ200/200 mice that does not affect spontaneous locomotion and motor coordination. Examples of dissociation between changes in HD biomarkers and behaviors were also reported for HdhQ150/+ and HdhQ200/+ mice, who do not exhibit motor deficits on the rotarod, even when studying HdhQ150/150 mice until 2 years of age (Heng et al., 2010, 2007). Thus, HdhQ200/200 mice represent a novel HD mouse model that recapitulates select components of HD pathogenesis by maintaining CAG copy numbers within the 200-copy range and exhibits a reduced life span and sex-dependent changes in the expression of HD biomarkers that do not systematically mirror impairment of locomotion and motor coordination (Pouladi et al., 2013).

It is known that significant sex-dependent differences exist in the molecular mechanisms that control the expansions and contractions of the CAG repeat on affected HD chromosomes in humans and that this mechanism occurs almost exclusively through paternal transmission (Kremer et al., 1995). Sex-dependent differences in the impaired behaviors of HD mouse models have been reported and are likely due to multiple molecular mechanisms. For example, sex-dependent reduced expression in regulators of chaperon Hsp70 activities, such as BAG1, and their ability to handle misfolding of mHtt have been reported in mice expressing the N171-82Q mutant (Orr et al., 2008). Thus, in this model that uses the mouse prion promoter to drive neuronal expression of N-terminal mHtt in all cells and independently of gender, male N171-82Q mice show a greater deficit in rotarod performance than female N171-82Q mice because of differences in the amounts of mHtt accumulation (Orr et al., 2008). Another example includes sex-dependent

deficiencies in insulin-like growth factor 1 receptors that affects mHtt aggregation by influencing autophagy and removal of mHtt (Corrochano et al., 2014). In the CAG_{N51} rat model of HD, sex-differences in pathogenesis are likely linked to decreased 17β-estradiol levels (Bode et al., 2008). In the HdhQ350/+ and BACHD mouse models, it is males that exhibit poorer motor coordination (Cao et al., 2018; Kuljis et al., 2016). Here, we found no overt differences in the CAG repeat length between sexes (Supplementary Fig. 1), indicating that the sex-dependent difference in HdhQ200/200 mice that we report is likely due to another mechanism. Our study provides a new example of sex-dependent impairment of behavior and pathological indices in HD mouse models.

HdhQ200/200 mice do not recapitulate several of the neuropathological biomarkers commonly studied to assess HD progression in striatal tissue. We show mHtt aggregation with no overt loss in MSN biomarkers (as measured by DARPP-32 and ENK expression) and in synaptic markers (CB_1R, vGLUT2, vGAT and PSD-95), all of which are down-regulated in human HD pathogenesis and in many HD mouse models (Glass et al., 1993; Goto and Hirano, 1990; Naydenov et al., 2014). It should be emphasized that we detected more mHtt-aggregated foci in HdhQ200/200 males than HdhQ200/200 females, and yet HdhQ200/200 males showed minor changes in locomotion and motor coordination, common indices measured in HD mouse models. This result aligns with results suggesting that mHtt-aggregated foci represent a defense mechanism to reduce the amount of toxic free soluble mHtt species (Saudou et al., 1998; Taylor et al., 2003). Specifically, the lower levels of insoluble mHtt detected in females may lead to higher levels of toxic soluble mHtt responsible for a more severe phenotype. A dissociation between behavioral deficits and neuropathology has also been previously described in the related HdhQ350/+ model (Cao et al., 2018). Thus, we provide a new example whereby pronounced behavioral impairments in mouse models of HD are not systematically associated with more HD aggregates.

We report an early-onset functional deficit in corticostriatal connectivity in female HdhQ200/200 mice, as evidenced by the *in vivo* $[Ca^{2+}]i$ imaging in MSNs at 8 months of age. The diverse and exaggerated calcium responses that we measured in MSNs of female HdhQ200/200 mice when stimulating the motor cortex indicate MSN hyperexcitability and can be interpreted in the context of electrophysiological recordings done in HD mice that led several laboratories to predict hyperexcitability and increase calcium entry in MSNs that disrupts their function (Cepeda et al., 2001; Levine et al., 1999; Starling et al., 2005; Zeron et al., 2004, 2002). Accordingly, extracellular single unit electrophysiological recordings in freely moving R6/2 mice showed dysregulated information processing by MSNs, as revealed by pairs of MSN populations that exhibited reduced correlated firing due to larger evoked EPSCs and decreased spontaneous IPSCs controlling layers II/III of cortical pyramidal neurons (Cummings et al., 2009; Miller et al., 2008). MSNs in the knock-in Q175 mouse line and TgCAG100 mice also become progressively more excitable with age, as demonstrated by robust changes in membrane resistance and rheobasic current measured by slice electrophysiology recording (Heikkinen et al., 2012). Remarkably, pre-pulse inhibition experiments show that the locus of synaptic dysfunction in Q175 mice is not due to pre- or post-synaptic changes in corticostriatal transmission and that post-synaptic AMPA receptor function was not impaired (Heikkinen et al., 2012). Whole-cell patch recording showed reduced cortical excitability in Q175 mice due to reduced excitatory and increased inhibitory inputs to striatal MSNs (Indersmitten et al., 2015). Altered excitatory and inhibitory inputs to pyramidal neurons in the cortex have also been reported for YAC128, BACHD and CAG140 knock-in mouse model, indicating that cortical dysfunction represents a prevailing deficit throughout the development of the disease whereby synaptic excitatory and inhibitory inputs onto cortical pyramidal neurons are differentially and sometimes opposite to those of striatal MSNs (Heikkinen et al., 2012; Spampanato et al., 2008). Thus, cortical dysfunction may contribute to the large-amplitude events detected in MSNs, and early dysfunction of the corticostriatal pathway may contribute to the behavioral deficits measured with the rotarod (Raymond, 2017). Together, these studies also emphasize the similarities and differences among HD mouse models where both hyperexcitability and hypoexcitability have been observed depending on the brain region often resulting in abnormal depolarizations and increases in $[Ca^{2+}]i$ in MSNs.

Several studies showed that mHtt expression in neurons dysregulate $[Ca^{2+}]i$ through several mechanisms, including increased expression of extrasynaptic NMDA receptors by MSNs, enhanced activity of store-operated calcium entry pathways and direct binding to IP_3R1 in MSNs (Duvernay et al., 2011; Miller and Bezprozvanny, 2010). While we did not detect changes in striatal Orai1 expression, we found significant reduction in GLT-1 expression in female HdhQ200/200 mice that coincided with increased calcium response in their MSNs, suggesting that reduction in astrocytic uptake of glutamate could be responsible for increased excitation of MSNs by cortical projections. We also found no evidence of overt reactive astrogliosis as measured by GFAP expression in HdhQ200/200 female mice at 8 months of age, suggesting that the molecular mechanism that links HdhQ200/200 expression to reduction in GLT-1 expression is selective and doesn't involve an overall change in astrocyte phenotype at that age. Interestingly, while astrogliosis is detected at later stages of disease progression in other HD mouse models, previous work has shown that astrocyte dysfunction through aberrant calcium and glutamate signaling occurs prior to detectable astrogliosis, similar to what we saw in the HdhQ200/200 mice (Faideau et al., 2010; Jiang et al., 2016). Thus, our results suggest that sex-dependent disruption in GLT-1 expression and other astrocytic biomarkers should be further explored as early indices of HD pathogenesis.

In conclusion, we show that the HdhQ200/200 mouse line replicates select aspects of HD pathogenesis and exhibits a reduced life span. The sex-dependent and early onset of impaired striatal-dependent behaviors detected in this model coincides with dysregulated changes in intracellular calcium levels of MSNs and reduced expression of striatal GLT-1, and are not associated with changes in MSN biomarkers commonly studied in other HD model systems. Thus, the HdhQ200/200 mouse line represents valuable model system to study select molecular mechanisms triggered by HD pathogenesis that result in early onset of impaired spontaneous locomotion, motor coordination and MSN function.

Declaration of Competing Interest

All authors report no conflict of interest.

Acknowledgements

The CHDD Behavioral Core and Dr. Toby Cole for advising and providing access to behavioral equipment. The CHDD Microscopy Center and Dr. Glenn MacDonald for advising and providing access to the Marianas Live Cell Imaging Microscope. Sofia Simonton Siegel for assistance with experiments. The work was supported by National Institutes of HealthDA026430 and NS98777 to NS and MH104450 to LZ.

Appendix A. Supplementary data

Supplementary data to this article can be found online at https://doi.org/10.1016/j.nbd.2019.104607.

References

Arzberger, T., Krampfl, K., Leimgruber, S., Weindl, A., 1997. Changes of NMDA receptor subunit (NR1, NR2B) and glutamate transporter (GLT1) mRNA expression in Huntington's disease—an in situ hybridization study. J. Neuropathol. Exp. Neurol. 56, 440–454.

Bode, F.J., Stephan, M., Suhling, H., Pabst, R., Straub, R.H., Raber, K.A., Bonin, M., Nguyen, H.P., Riess, O., Bauer, A., 2008. Sex differences in a transgenic rat model of Huntington's disease: decreased 17β-estradiol levels correlate with reduced numbers of DARPP32+ neurons in males. Hum. Mol. Genet. 17, 2595–2609.
Cao, J.K., Detloff, P.J., Gardner, R.G., Stella, N., 2018. Sex-dependent behavioral impairments in the HdhQ350/+ mouse line. Behav. Brain Res. 337, 34–45.
Cepeda, C., Ariano, M.A., Calvert, C.R., Flores-Hernández, J., Chandler, S.H., Leavitt, B.R., Hayden, M.R., Levine, M.S., 2001. NMDA receptor function in mouse models of Huntington disease. J. Neurosci. Res. 66, 525–539.
Corrochano, S., Renna, M., Osborne, G., Carter, S., Stewart, M., May, J., Bates, G.P., Brown, S.D., Rubinsztein, D.C., Acevedo-Arozena, A., 2014. Reducing Igf-1r levels leads to paradoxical and sexually dimorphic effects in HD mice. PLoS One 9, e105595.
Costa, R.M., Cohen, D., Nicolelis, M.A.L., 2004. Differential corticostriatal plasticity during fast and slow motor skill learning in mice. Curr. Biol. 1124–1134.
Cummings, D.M., André, V.M., Uzgil, B.O., Gee, S.M., Fisher, Y.E., Cepeda, C., Levine, M.S., 2009. Alterations in cortical excitation and inhibition in genetic mouse models of Huntington's disease. J. Neurosci. 29, 10371–10386.
Dou, Y., Xia, J., Gao, R., Gao, X., Munoz, F.M., Wei, D., Tian, Y., Barrett, J.E., Ajit, S., Meucci, O., et al., 2018. Orai1 plays a crucial role in central sensitization by modulating neuronal excitability. J. Neurosci. 38, 887–900.
Duvernay, M.T., Wang, H., Dong, C., Guidry, J.J., Sackett, D.L., Wu, G., 2011. Alpha2B-adrenergic receptor interaction with tubulin controls its transport from the endoplasmic reticulum to the cell surface. J. Biol. Chem. 286, 14080–14089.
Faideau, M., Kim, J., Cormier, K., Gilmore, R., Welch, M., Auregan, G., Dufour, N., Guillermier, M., Brouillet, E., Hantraye, P., et al., 2010. In vivo expression of polyglutamine-expanded huntingtin by mouse striatal astrocytes impairs glutamate transport: a correlation with Huntington's disease subjects. Hum. Mol. Genet. 19, 3053–3067.
Glass, M., Faull, R.L., Dragunow, M., 1993. Loss of cannabinoid receptors in the substantia nigra in Huntington's disease. Neuroscience 56, 523–527.
Goto, S., Hirano, A., 1990. Synaptophysin expression in the striatum in Huntington's disease. Acta Neuropathol. 80, 88–91.
Heikkinen, T., Lehtimäki, K., Vartiainen, N., Puoliväli, J., Hendricks, S.J., Glaser, J.R., Bradaia, A., Wadel, K., Touller, C., Kontkanen, O., 2012. Characterization of neurophysiological and behavioral changes, MRI brain volumetry and 1H MRS in zQ175 knock-in mouse model of Huntington's disease. PLoS One 7, e50717.
Heng, M.Y., Tallaksen-Greene, S.J., Detloff, P.J., Albin, R.L., 2007. Longitudinal evaluation of the Hdh(CAG)150 knock-in murine model of Huntington's disease. J. Neurosci. 27, 8989–8998.
Heng, M.Y., Duong, D.K., Albin, R.L., Tallaksen-Greene, S.J., Hunter, J.M., Lesort, M.J., Osmand, A., Paulson, H.L., Detloff, P.J., 2010. Early autophagic response in a novel knock-in model of Huntington disease. Hum. Mol. Genet. 19, 3702–3720.
Horne, E.A., Coy, J., Swinney, K., Fung, S., Cherry, A.E., Marrs, W.R., Naydenov, A.V., Lin, Y.H., Sun, X., Keene, C.D., et al., 2013. Downregulation of cannabinoid receptor 1 from neuropeptide Y interneurons in the basal ganglia of patients with Huntington's disease and mouse models. Eur. J. Neurosci. 37, 429–440.
Indersmitten, T., Tran, C.H., Cepeda, C., Levine, M.S., 2015. Altered excitatory and inhibitory inputs to striatal medium-sized spiny neurons and cortical pyramidal neurons in the Q175 mouse model of Huntington's disease. J. Neurophysiol. 113, 2953–2966.
Jiang, R., Diaz-Castro, B., Looger, L.L., Khakh, B.S., 2016. Dysfunctional calcium and glutamate signaling in striatal astrocytes from Huntington's disease model mice. J. Neurosci. 36, 3453–3470.
Kremer, B., Almqvist, E., Theilmann, J., Spence, N., Telenius, H., Goldberg, Y., Hayden, M., 1995. Sex-dependent mechanisms for expansions and contractions of the CAG repeat on affected Huntington disease chromosomes. Am. J. Hum. Genet. 57, 343.
Kuljis, D.A., Gad, L., Loh, D.H., Kaswan, Z.M., Hitchcock, O.N., Ghiani, C.A., Colwell, C.S., 2016. Sex differences in circadian dysfunction in the BACHD mouse model of Huntington's disease. PLoS One 11, e0147583.
Kumar, A., Zhang, J., Tallaksen-Greene, S., Crowley, M.R., Crossman, D.K., Morton, A.J., van Groen, T., Kadish, I., Albin, R.L., Lesort, M., et al., 2016. Allelic series of Huntington's disease knock-in mice reveals expression discorrelates. In: Human Molecular Genetics. Oxford University Press, pp. ddw040.
Landles, C., Bates, G.P., 2004. Huntingtin and the molecular pathogenesis of Huntington's disease. Fourth in molecular medicine review series. EMBO Rep. 5, 958–963.
Levine, M.S., Klapstein, G.J., Koppel, A., Gruen, E., Cepeda, C., Vargas, M.E., Jokel, E.S., Carpenter, E.M., Zanjani, H., Hurst, R.S., 1999. Enhanced sensitivity to N-methyl-D-aspartate receptor activation in transgenic and knockin mouse models of Huntington's disease. J. Neurosci. Res. 58, 515–532.
Lievens, J.C., Woodman, B., Mahal, A., Spasic-Boscovic, O., Samuel, D., Kerkerian-Le Goff, L., Bates, G.P., 2001. Impaired glutamate uptake in the R6 Huntington's disease transgenic mice. Neurobiol. Dis. 8, 807–821.
Lin, C.-H., Tallaksen-Greene, S., Chien, W.-M., Cearley, J.A., Jackson, W.S., Crouse, A.B., Ren, S., Li, X.-J., Albin, R.L., Detloff, P.J., 2001. Neurological abnormalities in a knock-in mouse model of Huntington's disease. In: Human Molecular Genetics. Oxford Univ Press, pp. 137–144.
Miller, B.R., Bezprozvanny, I., 2010. Corticostriatal circuit dysfunction in Huntington's disease: intersection of glutamate, dopamine and calcium. Future Neurol. 5, 735–756.
Miller, B.R., Walker, A.G., Shah, A.S., Barton, S.J., Rebec, G.V., 2008. Dysregulated information processing by medium spiny neurons in striatum of freely behaving mouse models of Huntington's disease. J. Neurophysiol. 100, 2205–2216.
Mitsui, K., Nakayama, H., Akagi, T., Nekooki, M., Ohtawa, K., Takio, K., Hashikawa, T., Nukina, N., 2002. Purification of polyglutamine aggregates and identification of elongation factor-1alpha and heat shock protein 84 as aggregate-interacting proteins. J. Neurosci. 22, 9267–9277.
Moccia, F., Zuccolo, E., Soda, T., Tanzi, F., Guerra, G., Mapelli, L., Lodola, F., D'Angelo, E., 2015. Stim and Orai proteins in neuronal Ca(2+) signaling and excitability. Front. Cell. Neurosci. 9, 153.
Naydenov, A.V., Sepers, M.D., Swinney, K., Raymond, L.A., Palmiter, R.D., Stella, N., 2014. Genetic rescue of CB1 receptors on medium spiny neurons prevents loss of excitatory striatal synapses but not motor impairment in HD mice. Neurobiol. Dis. 71, 140–150.
Orr, A.L., Huang, S., Roberts, M.A., Reed, J.C., Li, S., Li, X.-J., 2008. Sex-dependent effect of BAG1 in ameliorating motor deficits of Huntington disease transgenic mice. J. Biol. Chem. 283, 16027–16036.
Perego, C., Vanoni, C., Bossi, M., Massari, S., Basudev, H., Longhi, R., Pietrini, G., 2000. The GLT-1 and GLAST glutamate transporters are expressed on morphologically distinct astrocytes and regulated by neuronal activity in primary hippocampal co-cultures. J. Neurochem. 75, 1076–1084.
Pouladi, M.A., Morton, A.J., Hayden, M.R., 2013. Choosing an animal model for the study of Huntington's disease. Nat. Rev. Neurosci. 14, 708–721.
Prakriya, M., Feske, S., Gwack, Y., Srikanth, S., Rao, A., Hogan, P.G., 2006. Orai1 is an essential pore subunit of the CRAC channel. Nature 443, 230–233.
Raymond, L.A., 2017. Striatal synaptic dysfunction and altered calcium regulation in Huntington disease. Biochem. Biophys. Res. Commun. 483, 1051–1062.
Rogers, D.C., Fisher, E.M., Brown, S.D., Peters, J., Hunter, A.J., Martin, J.E., 1997. Behavioral and functional analysis of mouse phenotype: SHIRPA, a proposed protocol for comprehensive phenotype assessment. Mamm. Genome 8, 711–713.
Ross, C.A., Tabrizi, S.J., 2011. Huntington's disease: from molecular pathogenesis to clinical treatment. Lancet Neurol. 10, 83–98.
Saudou, F., Finkbeiner, S., Devys, D., Greenberg, M.E., 1998. Huntingtin acts in the nucleus to induce apoptosis but death does not correlate with the formation of intranuclear inclusions. Cell 95, 55–66.
Soden, M.E., Jones, G.L., Sanford, C.A., Chung, A.S., Guler, A.D., Chavkin, C., Lujan, R., Zweifel, L.S., 2013. Disruption of dopamine neuron activity pattern regulation through selective expression of a human KCNN3 mutation. Neuron 80, 997–1009.
Soloveva, M.V., Jamadar, S.D., Poudel, G., Georgiou-Karistianis, N., 2018. A critical review of brain and cognitive reserve in Huntington's disease. Neurosci. Biobehav. Rev. 88, 155–169.
Spampanato, J., Gu, X., Yang, X.W., Mody, I., 2008. Progressive synaptic pathology of motor cortical neurons in a BAC transgenic mouse model of Huntington's disease. Neuroscience 157, 606–620.
Squitieri, F., Gellera, C., Cannella, M., Mariotti, C., Cislaghi, G., Rubinsztein, D.C., Almqvist, E.W., Turner, D., Bachoud-Levi, A.C., Simpson, S.A., et al., 2003. Homozygosity for CAG mutation in Huntington disease is associated with a more severe clinical course. Brain 126, 946–955.
Starling, A.J., André, V.M., Cepeda, C., De Lima, M., Chandler, S.H., Levine, M.S., 2005. Alterations in N-methyl-D-aspartate receptor sensitivity and magnesium blockade occur early in development in the R6/2 mouse model of Huntington's disease. J. Neurosci. Res. 82, 377–386.
Steele, A.D., Jackson, W.S., King, O.D., Lindquist, S., 2007. The power of automated high-resolution behavior analysis revealed by its application to mouse models of Huntington's and prion diseases. Proc. Natl. Acad. Sci. U. S. A. 104, 1983–1988.
Steinbach, J.M., Garza, E.T., Ryan, B.C., 2016. Novel object exploration as a potential assay for higher order repetitive behaviors in mice. J. Vis. Exp. 114, 54324.
Sullivan, R., Rauen, T., Fischer, F., Wiessner, M., Grewer, C., Bicho, A., Pow, D.V., 2004. Cloning, transport properties, and differential localization of two splice variants of GLT-1 in the rat CNS: implications for CNS glutamate homeostasis. Glia 45, 155–169.
Svenningsson, P., Nishi, A., Fisone, G., Girault, J.A., Nairn, A.C., Greengard, P., 2004. DARPP-32: an integrator of neurotransmission. Annu. Rev. Pharmacol. Toxicol. 44, 269–296.
Taylor, J.P., Tanaka, F., Robitschek, J., Sandoval, C.M., Taye, A., Markovic-Plese, S., Fischbeck, K.H., 2003. Aggresomes protect cells by enhancing the degradation of toxic polyglutamine-containing protein. Hum. Mol. Genet. 12, 749–757.
Trottier, Y., Lutz, Y., Stevanin, G., Imbert, G., Devys, D., Cancel, G., Saudou, F., Weber, C., David, G., Tora, L., et al., 1995. Polyglutamine expansion as a pathological epitope in Huntington's disease and four dominant cerebellar ataxias. Nature 378, 403–406.
Walker, F.O., 2007. Huntington's disease. Lancet 218–228 (Elsevier).
Woltjer, R.L., Duerson, K., Fullmer, J.M., Mookherjee, P., Ryan, A.M., Montine, T.J., Kaye, J.A., Quinn, J.F., Silbert, L., Erten-Lyons, D., et al., 2010. Aberrant detergent-insoluble excitatory amino acid transporter 2 accumulates in Alzheimer disease. J. Neuropathol. Exp. Neurol. 69, 667–676.
Zeron, M.M., Hansson, O., Chen, N., Wellington, C.L., Leavitt, B.R., Brundin, P., Hayden, M.R., Raymond, L.A., 2002. Increased sensitivity to N-methyl-D-aspartate receptor-mediated excitotoxicity in a mouse model of Huntington's disease. Neuron 33, 849–860.
Zeron, M.M., Fernandes, H.B., Krebs, C., Shehadeh, J., Wellington, C.L., Leavitt, B.R., Baimbridge, K.G., Hayden, M.R., Raymond, L.A., 2004. Potentiation of NMDA receptor-mediated excitotoxicity linked with intrinsic apoptotic pathway in YAC transgenic mouse model of Huntington's disease. Mol. Cell. Neurosci. 25, 469–479.